RSC Advances

PAPER

View Article Online
View Journal | View Issue

Check for updates

Cite this: *RSC Adv.*, 2020, **10**, 15976

SCIP: a new simultaneous vapor phase coating and infiltration process for tougher and UV-resistant polymer fibers†

Itxasne Azpitarte,[a] Gabriele A. Botta,[a] Christopher Tollan[a] and Mato Knez *[ab]

Received 4th March 2020
Accepted 6th April 2020

DOI: 10.1039/d0ra02073g

rsc.li/rsc-advances

The physical properties of polymers can be significantly altered by blending them with inorganic components. This can be done during the polymerization process, but also by post-processing of already shaped materials, for example through coating by atomic layer deposition (ALD) or hybridizing through vapor phase infiltration (VPI), both of which are beneficial in their own way. Here, a new processing strategy is presented, which allows distinct control of the coating and infiltration. The process is a hybrid VPI and ALD process, allowing separate control of infiltrated and coated components. This new simultaneous vapor phase coating and infiltration process (SCIP) enhances the degrees of freedom for optimizing the properties of polymers, as shown on the example of Kevlar 29 fibers. The SCIP treated fibers show an increase of 17% of their modulus of toughness (MOT) in comparison to native Kevlar, through the nanoscale coating with alumina. At the same time their intrinsic sensitivity to 24 hours UV-irradiation was completely suppressed through another infiltrated material, zinc oxide, which absorbs the UV irradiation in the subsurface area of the fibers.

Open Access Article. Published on 22 April 2020. Downloaded on 1/18/2026 7:11:38 PM.
This article is licensed under a Creative Commons Attribution-NonCommercial 3.0 Unported Licence.

Introduction

Functional coatings can add value to the chemical or physical properties of polymers. Many different procedures have been studied to produce functional coatings on polymers and especially on polymeric fibers, which are of great interest for a great number of applications, including functional textiles, aeronautics, *etc.* Especially for polyamides several interesting examples of top–down modification have been shown in the recent years.[1,2] All these methods generally rely on an immobilization of dissimilar materials on a fiber's surface.

Among the most common issues related to the coating of the surface of a flexible material, such as a polymer, is frequently peeling-off of the coating or stiffening of the polymer. Such issues often result from a mismatch between the young's modulus of the polymer and the coating. One way to reduce this mismatch is to avoid an abrupt interface between the polymer and the coating. This can be achieved by blending the dissimilar materials and creation of a hybrid materials layer.

Approaches to create hybrid materials are manifold. While many of them rely on blending polymers with inorganic particles during polymerization, molding or extrusion,[3,4] others focus on the fine dispersion of ionic inorganics, thus forming a true organic–inorganic network. Among the parade examples are metal–organic frameworks (MOFs),[5] which show a true hybrid nature and often exciting properties, which none of the individual components do. Most of those approaches, however, rely on bottom–up construction, meaning that they blend the materials upon formation. Once the polymer is shaped, typically such hybrid materials cannot be formed anymore, but they are rather coated with the inorganics.

However, recent research has shown some possible strategies towards top–down fabrication of hybrid materials, which rely on the infiltration of small molecules into the subsurface of the polymers, thereby resulting in a hybrid layer between the coating and the polymer bulk. However, the possibility of generating such a hybrid layer is strongly dependent on the applied technique and the functionality and density of the polymer. Highly dense polymers, such as Kevlar, limit the possibilities of an infiltration of molecules into the bulk.[6]

Generally, several methods can be used to infiltrate polymers from the liquid phase, but those require polymers with a high level of porosity in which the guest material can penetrate, aggregate and form clusters.[7] If a modification of the mechanical properties is aimed, then such clustering will most likely embrittle the polymer.

As efficient alternative to solution-based methods vapor phase techniques have proven being advantageous for achieving an incorporation of metals into polymers and in this way resulting in the fabrication of hybrid materials with improved mechanical properties.[8–10] The recently developed vapor phase infiltration (VPI) process offers a pathway to

[a]*CIC nanoGUNE BRTA, Tolosa Hiribidea 76, 20018, Donostia-San Sebastián, Spain. E-mail: m.knez@nanogune.eu*

[b]*IKERBASQUE, Basque Foundation for Science, 48011, Bilbao, Spain*

† Electronic supplementary information (ESI) available: Kevlar samples, Weibull analysis and infrared spectra. See DOI: 10.1039/d0ra02073g

This journal is © The Royal Society of Chemistry 2020

Open Access Article. Published on 22 April 2020. Downloaded on 1/18/2026 7:11:38 PM.
This article is licensed under a Creative Commons Attribution-NonCommercial 3.0 Unported Licence.

hybridize polymeric substrates with inorganic materials even after the final shape has been fabricated.[11]

VPI is derived from atomic layer deposition (ALD),[12,13] a vapor phase coating methodology based on sequential exposure of a substrate to two reactants (precursors), with intermediate purging steps. During the process the first precursor binds to a substrate forming an immobilized layer of highly reactive molecules. The subsequent purge and exposure to the second precursor ensures a reaction with the immobilized reactant and formation of one layer of the coat. Repeating this cycle results in the growth of a film with its thickness evolving as function of the number of applied cycles. Key is the chemical binding of the precursor to available anchoring sites of the substrate, regardless of its morphology, as long as the precursor vapors can access the anchoring sites.[14]

VPI bases on the same strategy but it applies to polymeric substrates where the precursors not only bind to the surface, but also diffuse into the polymer through a vapor–solid dissolution process.[15] In this way an inorganic–organic hybrid material will be formed in the subsurface area of the substrate. The depth of this infiltrated area can be modified by changing the exposure times, but it also can vary in dependence on the diffusivity of the precursors inside the polymer or the polymer's density.[16] However, since the same chemical functionalities are present also at the surface of the polymer, VPI will simultaneously generate a hybrid layer and a parasitic inorganic coating.

In this work we introduce the simultaneous vapor phase coating and infiltration process (SCIP), which makes it possible to coat and infiltrate a polymer with two distinct materials in the same process. On the example of Kevlar fibers we show that SCIP has an added value over the individual ALD and VPI processes, simultaneously increasing the toughness and eliminating the sensitivity of the material to UV light, which was not possible to achieve otherwise. Both, coating and infiltration can be achieved in the same run, thus the processing of such hybrid materials becomes simplified by applying SCIP.

Experimental section

Sample preparation

Kevlar fibers were obtained from the woven commercially used in bulletproof vests (Kevlar 29).

During every ALD process, two different types of samples were processed (Fig. S1 and S2 in the ESI†).

For mechanical testing an array of 20 individual fibers for each process was attached to a glass slide and further processed.

For FTIR characterization the woven, cut to approximately 1 × 1 cm in size with 0.3 mm thickness, was used.

All modifications of the samples were performed in a commercial ALD reactor (Savannah S100, Cam-bridge Nano-Tech Inc). Both infiltration and coating of the fibers were carried out at 150 °C under a constant nitrogen gas flow of 20 standard cubic centimeters per minute (sccm). Trimethylaluminum (TMA, $Al(CH_3)_3$, Strem Chemicals) was used as the aluminum source, diethylzinc (DEZ, $Zn(C_2H_5)_2$) was used as zinc source, and demineralized water as the oxygen source. The coated fibers were prepared following a typical ALD process with a cycle consisting of pulse(TMA, 0.08 s)/purge(N_2, 30 s)/pulse(H_2O, 0.08 s)/purge(N_2, 30 s). In contrast, the infiltrated fibers were prepared by VPI. Here, the substrate was exposed to the precursors for defined periods of time before purging, thereby allowing diffusion of the precursors into the polymer. A VPI cycle consisted of pulse(TMA, 0.08 s)/exposure(30 s)/purge(N_2, 30 s)/pulse(H_2O, 0.08 s)/exposure(30 s)/purge(N_2, 30 s). Finally, for the preparation of the sample coated with alumina and infiltrated with ZnO a combination of ALD and VPI was used. Each cycle consisted of pulse (TMA, 0.08 s)/purge(N_2, 30 s)/pulse(DEZ, 0.08 s)/exposure(30 s)/purge(N_2, 30 s)/pulse(H_2O, 0.08 s)/exposure(30 s)/purge(N_2, 30 s). In all cases, the number of repetitive ALD/VPI cycles was 200. The process schematic referring to ALD, VPI and SCIP processes can be found in Fig. S3 in the ESI.†

TEM/EDS

TEM characterization and EDS analyses were carried out with a FEI Titan microscope using 300 kV in STEM mode and an EDAX SDD detector.

FIB lamellae were prepared by gently stretching the Kevlar fibers across a convex aluminum SEM stub (prepared in-house) and fixing both ends of the fibers with carbon tape. Once the location for the block extraction was chosen, the fiber was locally fixed to the substrate with deposited Pt and a block was extracted by standard methods. A Pt electron beam deposition was initially used to protect the sample surface before any ion beam deposition was carried out. The block was thinned to transparency on a copper "Omniprobe" grid using a 5 kV gallium ion beam at 8 pA for final surface preparation.

Tensile tests

The tensile tests were done with a BRUKER Universal Mechanical Tester with a resolution of 50 μN and in accordance to the ASTM standard C1557-03 (2008). The fibers were fixed to a cardboard sampler holder, which had a punched hole of 6 mm diameter in the center. After vertical alignment of the fiber across the hole and fixation, the sample holder was positioned in the mechanical tester with the fiber being un-strained. Finally, the sample holder was cut along the central guides and tensile force was applied until rupture of the fiber, while the strain was measured simultaneously. To determine the stability of the fibers under UV light the samples were exposed to light with a wavelength of 365 nm for 24 hours. Subsequently, the strain–stress curves were measured and compared with the mechanical properties of unexposed fibers.

SEM

The morphology of the fibers after the tensile tests was analyzed by SEM. The SEM micrographs were taken in an environmental scanning electron microscope Quanta 250 FEG with a large field detector (LFD). The ruptured fibers were glued to a carbon tape and the images were taken at 10 kV and 70 Pa.

Open Access Article. Published on 22 April 2020. Downloaded on 1/18/2026 7:11:38 PM.
This article is licensed under a Creative Commons Attribution-NonCommercial 3.0 Unported Licence.

Attenuated total reflectance-Fourier transformed infrared spectroscopy (ATR-FTIR)

The FTIR spectra of the samples were acquired with a PerkinElmer Frontier spectrometer with an ATR sampling stage equipped with diamond/zinc selenide ATR crystal. All spectra were measured collecting 20 scans in the range from 520 cm^{-1} to 4000 cm^{-1} with 1 cm^{-1} resolution. Each sample was measured 5 times and the results were averaged.

X-ray diffraction (XRD)

The XRD spectra of the samples were measured with a PANalytical X'Pert Pro diffractometer with Cu-Kα radiation.

Results and discussion

In earlier works we demonstrated that the thermal and UV sensitivity of Kevlar can be suppressed by VPI of ZnO. Even though we did not achieve enhancement of the toughness of Kevlar, the loss in the modulus of toughness (MOT) upon thermal treatment and irradiation with UV light was limited to 10%.[17]

To increase the MOT, we explored coating and infiltration of Kevlar with Al_2O_3, since the precursor, trimethylaluminum (TMA), shows stronger Lewis-acidity than the precursor for ZnO (diethylzinc, DEZ), promising better reactivity with the polymeric substrate. Also, Al_2O_3 appears better suitable for target applications in flexible devices, since ALD-deposited alumina is amorphous, while ZnO tends to develop a more brittle nano- or polycrystalline wurtzite structure. The cross-sectional TEM images show that the structures of the samples strongly depend on the applied process (Fig. 1). Sample C-Al_2O_3 refers to alumina-coated Kevlar fibers processed following the ALD scheme reported in Fig. S3A.† A sharp and clear interface between the coating and the substrate can be observed (Fig. 1A). Generally, a growth of a film by ALD relies on covalent binding of the precursors to the substrate's surface, which results in great conformality and stability of the film against delamination even after mechanical bending. Similarly, an alumina thin film is grown on the surface of the alumina-VPI (I-Al_2O_3) sample, resulting from a process as schematically shown in Fig. S3B.† In this case, the extended exposure of the substrate to the precursors will enable their diffusion into the subsurface of the polymer, resulting in the formation of a less dense Al_2O_3-Kevlar hybrid layer underneath the coating (Fig. 1B). Note that a separation of coating and infiltrate during VPI is only possible by altering the chemistry of the substrate. Namely, with the same chemical functionalities on the surface and in the bulk of the polymer an infiltration and coating with the same materials will happen simultaneously.

Simultaneous vapor phase coating and infiltration (SCIP)

A workaround is possible through merging both processes into one so that the pulsing sequence allows for targeting coating and infiltration with two different materials. We developed SCIP, a hybrid of ALD and VPI, with a pulsing procedure as illustrated in Fig. S3C.† The process starts with an ALD-type

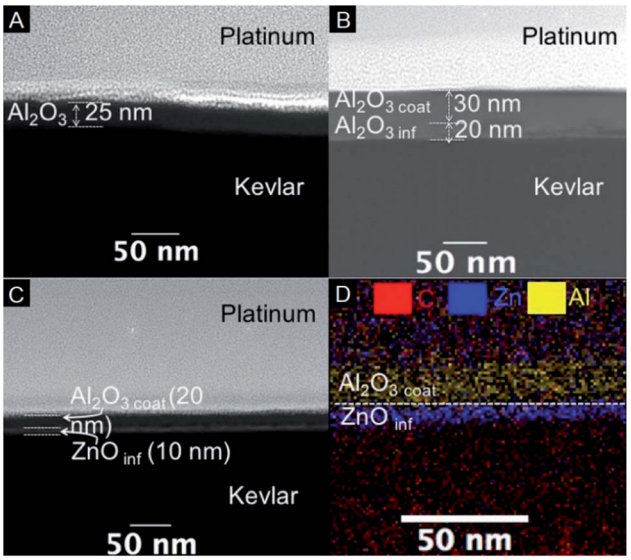

Fig. 1 TEM images of FIB-prepared cross-sections of (A) alumina-coated Kevlar (C-Al_2O_3), (B) alumina-infiltrated Kevlar (I-Al_2O_3), and (C) Kevlar coated with alumina and infiltrated with ZnO (SCIP). Platinum was deposited on top of the fibers for protecting the samples from damage during the ion beam sectioning and thinning and to obtain a precise cross-section cut. (D) EDS color map of the SCIP sample. EDS mapping did not show any presence of Zn in the Al_2O_3 coating, meaning that a potential intermixture of ZnO and Al_2O_3 is below the detection limit of the spectrometer.

pulse of TMA, a short pulse of the precursor without extended exposure time, which is followed by a purge step. Here, the TMA covalently binds to the surface of the fiber but is not hydrolyzed yet, thus it does not expose binding sites for further molecules.

Given that the diffusion of gaseous species into tightly packed polymers such as Kevlar is strongly dependent on the diffusion (*viz.* exposure) time, the use of short pulses with no nominal exposure time, followed by purge, will ensure that the infiltration of TMA into the polymer is negligible.[18] For the coating step of SCIP, the use of a precursor with rapid reaction kinetics with the Lewis base sites of the substrate ensures rapid surface saturation. In fact, is reported that the time needed to deposit a homogeneous monolayer of Al_2O_3 by ALD is approximately a third of that needed for a deposition of ZnO.[19]

Following this procedure, TMA binds to the surface and acts as inhibitor for the adsorption of the next precursor by occupying functional sites at the polymer surface. This first ALD-type of pulse is followed by a VPI-type of pulse, which consists of an exposure of the substrate to DEZ for an extended time period. As the superficial functional groups are saturated with TMA, the DEZ cannot bind to the surface, but diffuses into the fiber and reacts with the functional groups in the subsurface area of the polymer. For choosing the precursor for the infiltration step of a SCIP process, one important factor that must be considered is the relative reactivity with respect to the previously pulsed precursors. Namely, given that the VPI step is temporally extensive, etching or desorption might take place, if precursors compete for adsorption sites with an energetically more favorable bonding or if they react with each other. In our case, DEZ is

 This journal is © The Royal Society of Chemistry 2020

Open Access Article. Published on 22 April 2020. Downloaded on 1/18/2026 7:11:38 PM.
This article is licensed under a Creative Commons Attribution-NonCommercial 3.0 Unported Licence.

an excellent choice as VPI precursor, because it won't etch the surface-chemisorbed TMA given the lower formation enthalpy of ZnO (-353 kJ mol^{-1}) compared to Al_2O_3 (-845 kJ mol^{-1}).[20,21] In this way a clear separation of the surface-bound TMA and the subsurface bound DEZ is achieved, driven by the chemical saturation of the available binding sites in each case. A final exposure to water vapor hydrolyzes both the surface-bound TMA and the infiltrated DEZ to generate the respective metal oxides. The resulting "SCIP" sample expectedly shows such a sophisticated construction. Namely, two different metal oxides are present, Al_2O_3 as an amorphous thin film on the surface of the fiber and ZnO as the inorganic component of the hybrid material created in the subsurface of the polymer (Fig. 1C and D).

Mechanical properties

After performing tensile tests with the fibers and calculating their MOT, all processed samples show an increase in comparison to native Kevlar (Fig. 2A). This effect can be ascribed to the alumina coating grown on each sample upon coating or infiltration, which stiffens the polymeric fiber, consequently increasing the Young's modulus and the Ultimate Tensile Strength (UTS), *viz* the MOT. However, the stress–strain curves in Fig. 2B show differences among the samples. In C-Al_2O_3, the MOT increases by 13%, but the failure strain is significantly reduced in comparison to native Kevlar. In contrast, the curve of I-Al_2O_3 largely resembles that of untreated Kevlar with an increased MOT of only 5%. Based on earlier evidence highlighted by the research of Spagnola and Parsons groups,[22,23] together with our cross-sectional TEM investigations (Fig. 1B), it can be stated that precursor TMA can degrade the polymer. A porous Al_2O_3 film is found at the interface of the coating and the polymer, this area is likely an initially infiltrated and subsequently degraded part of the subsurface area of Kevlar. Thus, the I-Al_2O_3 sample dominantly reflects the characteristic high rupture strain of the Kevlar.

Significant improvement is observed from the "SCIP" sample, where the MOT increases by 17%. This improvement results from the increase of the Young's Modulus and UTS and a higher failure strain. The sample consists of ZnO infiltrated into the subsurface area of Kevlar and an additional coating with Al_2O_3. The greatly increased MOT indicates that the Kevlar-ZnO hybrid acts as an ideal interface, covalently binding the alumina film to the polymeric substrate. At the same time, it is flexible enough to compensate the stress occurring from the differences in flexibility between the inorganic coating and the flexible polymer. The significance of the differences observed among the fibers was confirmed by a two-tailed test. The obtained low p-value ($p = 0.0013$) confirms that the improvement of the MOT in the treated samples is statistically significant and not a simple variation of the average value.

One of the main drawbacks of Kevlar is its poor UV stability. Metal oxides may meet this issue as they can absorb UV light, protecting the underlying polymer. With this respect the mechanical properties of the coated and infiltrated samples were analyzed after exposing the fibers to UV light for 24 hours. Fig. 2A shows that the untreated Kevlar maintains only 45% of its MOT after exposure. The I-Al_2O_3 and C-Al_2O_3 samples show higher UV resistance, maintaining 65% of their MOT. The SCIP sample, however, outperforms both samples, maintaining 100% of the MOT.

The SCIP sample takes advantage from the added value of two materials; the infiltrated ZnO as an excellent UV-light absorber and the Al_2O_3 coating as enhancer of the MOT. The reliability of the mechanical property measurements is assessed by means of a Weibull distribution analysis and the most

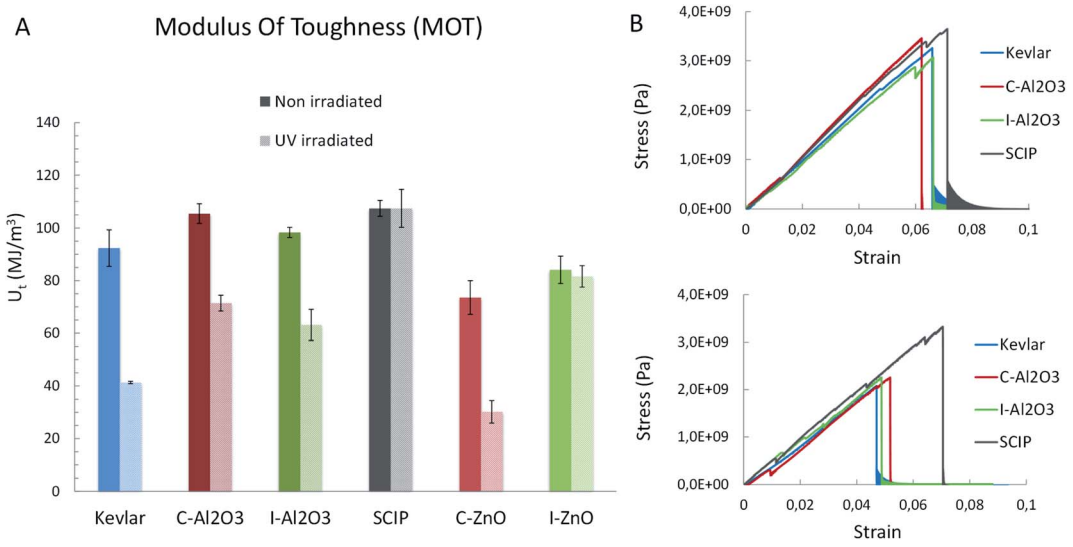

Fig. 2 Mechanical properties comparison. Comparison of the mechanical properties of untreated Kevlar fibers and fibers after infiltration (I-Al_2O_3) or coating (C-Al_2O_3) with Al_2O_3 and after infiltration with ZnO and simultaneous coating with Al_2O_3 (SCIP). (A) Modulus of toughness before and after irradiation with UV light (all values are averaged from 7 samples and the error bars correspond to the standard error) C-ZnO and I-ZnO refer to sample processed in earlier work,[6] and (B) stress–strain curves before and after irradiation with UV light.

Open Access Article. Published on 22 April 2020. Downloaded on 1/18/2026 7:11:38 PM.
This article is licensed under a Creative Commons Attribution-NonCommercial 3.0 Unported Licence.

important parameters are summarized in Table S1.† The large variation found in the results from these fibers reveals that the failure causing defects are not homogeneously distributed or inconsistently clustered throughout the material. The inhomogeneous distribution of the flaws might be due to the UV induced degradation preferentially occurring at the Kevlar-Al_2O_3 interface as a result of TMA-induced degradation. An analysis of the fracture area shows that the failure of Kevlar fibers is mainly caused by fibrillation and splitting along the fiber axis (Fig. 3) in agreement with literature.[24,25] The ruptures of the untreated fiber start at an imperfection on the surface. The longitudinal shear stresses, induced at the initial imperfection, cause longitudinal splitting of the first bundle of fibrils. The tensile modulus and strength are much higher than the shear modulus and strength resulting in the crack developing under a steep angle. The break is further transmitted from one fibrillar unit to another until the filament is broken completely.[26] The UV-irradiated sample, in contrast, shows negligible fibrillation, characteristic of a brittle fracture mode. It is explained by UV induced polymer chain scission reactions resulting in weakening of the tensile modulus and strength of the fiber. Thus, the initial crack develops perpendicular to the fiber axis and propagates until complete failure of the filament. The same fracture mode is observed from the C-Al_2O_3 and I-Al_2O_3 Kevlar samples after UV exposure, showing that the alumina infiltration obviously does not prevent the UV-induced degradation of Kevlar. In contrast, the SCIP sample shows the fibrillar type of fracture. The longitudinal splitting and the fibrillation show that the combination of alumina coating and ZnO infiltration does not significantly embrittle the fiber.

Characterization

The chemical changes induced by the processes were characterized by infra-red spectroscopy. We applied attenuated total reflectance Fourier-transform infrared spectroscopy (ATR)-FTIR, which is very convenient for the characterization of the near surface region of the samples (Fig. S2†). The most pronounced differences among the samples are seen in the fingerprint area, specifically in the region between 950 cm^{-1} and 1000 cm^{-1} (Fig. 4A), where stretching signatures of C–N, C–O and C–C bonds appear. A peak at 940 cm^{-1} in the spectra of the C-Al_2O_3 and I-Al_2O_3 samples indicates the development of C–O single bonds, a result of binding of the Lewis acid TMA to the oxygen of the C═O bond in the amide.

An additional peak develops around 960 cm^{-1}, which can be assigned to C–C stretching, indicating newly developing C–C bonds. The intensity of that peak in the SCIP sample is low, likely showing a moderate level of chemical modification, while it is stronger in the two Al_2O_3-coated and infiltrated samples. A newly forming C–C bond in C-Al_2O_3 and I-Al_2O_3 results from the nucleophilic attack of the released methyl ligand of TMA on the carbonyl C in the amide, resulting in splitting of the amidic C–N bond and formation of a new C–C bond (Fig. 4B). Native Kevlar and the SCIP sample show a pronounced peak at 980 cm^{-1}, a signature of C–N bonds, which has nearly vanished in the I-Al_2O_3 and C-Al_2O_3 samples. At higher wavenumbers, shifts in the amide peaks confirm that the infiltrated precursors interact with the amide groups. The individual wavenumbers of these peaks are depicted in Table S2† for easier comparison. While the alumina coating does not significantly alter the spectral signature of Kevlar, the infiltration and SCIP do. Both processes affect the N–H and C═O (amide I) bonds, which constitute the hydrogen bonds between the polymer chains. The blue shift of the amide II and amide III peaks indicates that both metals interact with the nitrogen, as those peaks are related to the C–N bond stretching. The shift is more strongly expressed after infiltration of ZnO, indicating stronger bonding of Zn to the N and a resulting alteration of the C–N bonding strength. The ZnO infiltration (SCIP sample) has a stronger impact on the N–H bonds than the Al_2O_3 infiltration (I-Al_2O_3 sample), while with the amide I, the situation is reverse. This is in-line with the observations from the fingerprint area where Al is more efficiently binding to C═O than Zn, which on the other hand has a stronger affinity to N–H than Al.[27] Thus, in agreement with the conclusions extracted from the mechanical data, the alumina processes are more strongly degrading the polymer chains, while covalent cross-linking of the Kevlar chains is more pronounced in the SCIP sample, which is further confirmed with X-ray diffraction (Fig. 4C). The crystallographic features of the samples by X-ray diffraction confirm the cross-linking ability of the infiltrated ZnO. Namely, the peaks indexed as [110] and [200] reflections of Kevlar shift to slightly lower angles after infiltration with ZnO, indicative of an increase of the interchain distance, likely resulting from insertion of ZnO into the material thereby cross-linking the polymer chains. The shift of the [211] reflection points towards a decrease of the stacking density of the crystallites. In contrast, the C-Al_2O_3 shows no alteration of the interchain spacing, but only a decrease in the stacking density. The I-Al_2O_3 sample shows in both aspects the opposite behavior, namely a decrease of the interchain spacing and an increase in the packing density, which presumably results from the molecular distortion upon chain scission and re-packing of the molecules within the fibers.

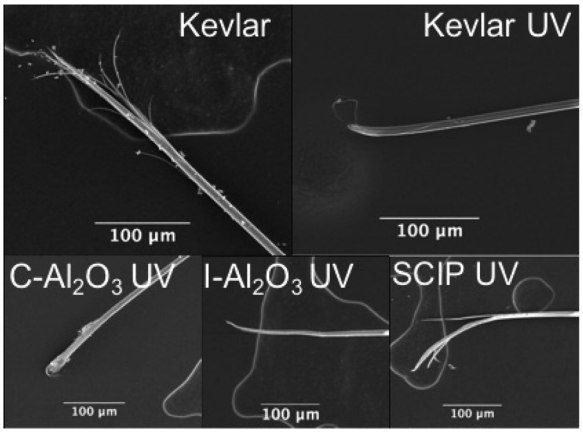

Fig. 3 SEM images of the broken ends of native, coated and infiltrated Kevlar samples after irradiation with UV light in comparison to Kevlar before irradiation. The broken terminals of the fibers indicate the fracture mode being fibrillar or brittle, in dependence on the pre-treatment being coating or infiltration.

 This journal is © The Royal Society of Chemistry 2020

Open Access Article. Published on 22 April 2020. Downloaded on 1/18/2026 7:11:38 PM.
This article is licensed under a Creative Commons Attribution-NonCommercial 3.0 Unported Licence.

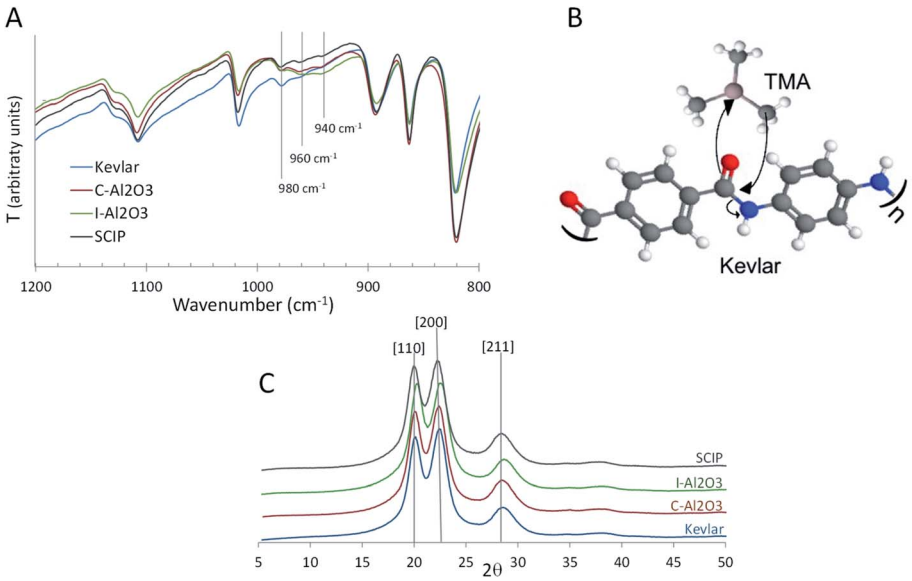

Fig. 4 Degradation of Kevlar due to alumina infiltration. (A) Fingerprint area (1200–800 cm^{-1}) of the ATR-FTIR spectra of Kevlar fibers before and after coating and infiltration. A peak at 940 cm^{-1} in the spectra of the C-Al_2O_3 and I-Al_2O_3 samples indicates the development of C–O single bonds, a result of binding of the Lewis acid TMA to the oxygen of the C=O bond in the amide. An additional peak develops around 960 cm^{-1}, which can be assigned to C–C stretching, indicating newly developing C–C bonds. The intensity of that peak in the SCIP sample is low, likely showing a moderate level of chemical modification, while it is stronger in the two Al_2O_3-coated and infiltrated samples. (B) Schematic view of the proposed reaction mechanism between Kevlar and TMA based on the FTIR data. (C) XRD diffraction patterns of the samples.

To understand how the structure of different samples is affected by UV light, FTIR spectra of the samples were measured after UV irradiation. No significant changes are noted in the shifts of the peaks, but rather in the intensities. In Table S3† the intensities of the peaks of the irradiated samples were normalized (Fig. S2†) and compared to those of the non-irradiated samples. In contrast to Kevlar, C-Al_2O_3 and I-Al_2O_3, the SCIP sample shows only negligible changes in the FTIR spectrum. Apparently, chain-scission reactions become less probable due to the high cross-linking level obtained by infiltrating ZnO, while simultaneously ZnO clusters buried inside the fiber absorb UV light, thus preventing degradation of the polymeric core.

Conclusions

Our hybrid coating and infiltration process SCIP allows a higher-level control of the functionalization of polymers. The separate control of thin film coating and infiltration within the same process gives access to altering both mechanical and optical properties of polymers within the same run. The merits of this method are shown on the SCIP sample processed at 150 °C for 200 cycles. The SCIP treated Kevlar fibers have shown a gain of 17% in the MOT. Thanks to the ZnO, infiltrated in the subsurface of the SCIP sample, the MOT persists even after 24 hours of exposure to UV light. ZnO is efficiently absorbing UV radiation, thus preventing a UV-induced degradation of the polymer. ALD and VPI-suitable chemical precursors are available for most metals, semimetals and semiconductors in the periodic system of elements. Those have varying physical properties including optical, mechanical or electronic properties. Upon exploring further material-substrate combinations we foresee great progress in the polymer-based materials research, as the processes can easily be upscaled to the industrial level and therefore are not only of scientific interest but can easily become economically meaningful.

Conflicts of interest

There are no conflicts to declare.

Acknowledgements

M. K. is grateful for funding from the Spanish Ministry of Economy and Competitiveness (MINECO) [Grant Agreement No. MAT2016-77393-R], including FEDER funds, and the Maria de Maeztu Units of Excellence Programme [grant number MDM-2016-0618]. The authors acknowledge networking support within the COST action HERALD [grant number MP1402]. I. A. acknowledges the Basque Government for a PhD fellowship [grant number PRE2016_2_0022] and G. B. acknowledges the Spanish Government for a PhD fellowship [grant number PRE2018_084190].

Notes and references

1 J. Gao, C. Huang, Y. Lin, P. Tong and L. Zhang, *In situ* solvothermal synthesis of metal-organic framework coated fiber for highly sensitive solid-phase microextraction of polycyclic aromatic hydrocarbons, *J. Chromatogr. A*, 2016, **1436**, 1–8.

Open Access Article. Published on 22 April 2020. Downloaded on 1/18/2026 7:11:38 PM. This article is licensed under a Creative Commons Attribution-NonCommercial 3.0 Unported Licence.

2 O. Rodríguez-Uicab, F. Avilés, P. I. Gonzalez-Chi, G. Canché-Escamilla, S. Duarte-Aranda, M. Yazdani-Pedram, P. Toro, F. Gamboa, M. A. Mazo, A. Nistal and J. Rubio, Deposition of carbon nanotubes onto aramid fibers using as-received and chemically modified fibers, *Appl. Surf. Sci.*, 2016, **385**, 379–390.

3 A. Sellinger, P. M. Weiss, A. Nguyen, Y. Lu, R. A. Assink, W. Gong and C. J. Brinker, Continuous self-assembly of organic–inorganic nanocomposite coatings that mimic nacre, *Nature*, 1998, **394**, 256–260.

4 L. Wang, Z. Zhang, Y. Liu, B. Wang, L. Fang, J. Qiu, K. Zhang and S. Wang, Exceptional thermoelectric properties of flexible organic–inorganic hybrids with monodispersed and periodic nanophase, *Nat. Commun.*, 2018, **9**, 1–8.

5 O. M. Yaghi, A tale of two entanglements, *Nat. Mater.*, 2007, **6**, 92–93.

6 R. P. Padbury and J. S. Jur, Systematic study of trimethyl aluminum infiltration in polyethylene terephthalate and its effect on the mechanical properties of polyethylene terephthalate fibers, *J. Vac. Sci. Technol., A*, 2015, **33**, 01A112.

7 Y. Zhang, M. Qiu, Y. Yu, B. Wen and L. Cheng, A novel polyaniline-coated bagasse fiber composite with core-shell heterostructure provides effective electromagnetic shielding performance, *ACS Appl. Mater. Interfaces*, 2017, **9**, 809–818.

8 C. D. McClure, C. J. Oldham and G. N. Parsons, Effect of Al_2O_3 ALD coating and vapor infusion on the bulk mechanical response of elastic and viscoelastic polymers, *Surf. Coat. Technol.*, 2015, **261**, 411–417.

9 K. Gregorczyk and M. Knez, Hybrid nanomaterials through molecular and atomic layer deposition: top down, bottom up, and in-between approaches to new materials, *Prog. Mater. Sci.*, 2016, **75**, 1–37.

10 S.-M. Lee, E. Pippel, U. Gösele, C. Dresbach, Y. Qin, C. V. Chandran, T. Bräuniger, G. Hause and M. Knez, Greatly Increased Toughness of Infiltrated Spider Silk, *Science*, 2009, **324**, 488–492.

11 W. Wang, F. Yang, C. Chen, L. Zhang, Y. Qin and M. Knez, Tuning the Conductivity of Polyaniline through Doping by Means of Single Precursor Vapor Phase Infiltration, *Adv. Mater. Interfaces*, 2017, **4**, 1–8.

12 A. Subramanian, N. Tiwale and C. Y. Nam, Review of Recent Advances in Applications of Vapor-Phase Material Infiltration Based on Atomic Layer Deposition, *Jom*, 2019, **71**, 185–196.

13 S. Lee, E. Pippel and M. Knez, Metal Infiltration into Biomaterials by ALD and CVD: A Comparative Study **, *Chem.–Eur. J.*, 2011, **12**, 791–798.

14 G. T. Hill, D. T. Lee, P. S. Williams, C. D. Needham, E. C. Dandley, C. J. Oldham and G. N. Parsons, Insight on the Sequential Vapor Infiltration Mechanisms of Trimethylaluminum with Poly(methyl methacrylate), Poly(vinylpyrrolidone), and Poly(acrylic acid), *J. Phys. Chem. C*, 2019, **123**, 16146–16152.

15 C. Z. Leng and M. D. Losego, Vapor phase infiltration (VPI) for transforming polymers into organic-inorganic hybrid materials: a critical review of current progress and future challenges, *Mater. Horiz.*, 2017, **4**, 747–771.

16 H. I. Akyildiz, R. P. Padbury, G. N. Parsons and J. S. Jur, Temperature and exposure dependence of hybrid organic-inorganic layer formation by sequential vapor infiltration into polymer fibers, *Langmuir*, 2012, **28**, 15697–15704.

17 I. Azpitarte, A. Zuzuarregui, H. Ablat, L. Ruiz-Rubio, A. López-Ortega, S. D. Elliott and M. Knez, Suppressing the Thermal and Ultraviolet Sensitivity of Kevlar by Infiltration and Hybridization with ZnO, *Chem. Mater.*, 2017, **29**, 10068–10074.

18 C. Z. Leng and M. D. Losego, Vapor phase infiltration (VPI) for transforming polymers into organic-inorganic hybrid materials: a critical review of current progress and future challenges, *Mater. Horiz.*, 2017, **4**, 747–771.

19 T. Homola, V. Buršíková, T. V. Ivanova, P. Souček, P. S. Maydannik, D. C. Cameron and J. M. Lackner, Mechanical properties of atomic layer deposited Al_2O_3/ZnO nanolaminates, *Surf. Coat. Technol.*, 2015, **284**, 198–205.

20 A. Illiberi, R. Scherpenborg, Y. Wu, F. Roozeboom and P. Poodt, Spatial atmospheric atomic layer deposition of alxzn1-xo, *ACS Appl. Mater. Interfaces*, 2013, **5**, 13124–13128.

21 J. S. Na, Q. Peng, G. Scarel and G. N. Parsons, Role of gas doping sequence in surface reactions and dopant incorporation during atomic layer deposition of Al-doped ZnO, *Chem. Mater.*, 2009, **21**, 5585–5593.

22 J. C. Spagnola, B. Gong, S. A. Arvidson, J. S. Jur, S. A. Khan and G. N. Parsons, Surface and sub-surface reactions during low temperature aluminium oxide atomic layer deposition on fiber-forming polymers, *J. Mater. Chem.*, 2010, **20**, 4213–4222.

23 G. N. Parsons, S. E. Atanasov, E. C. Dandley, C. K. Devine, B. Gong, J. S. Jur, K. Lee, C. J. Oldham, Q. Peng, J. C. Spagnola and P. S. Williams, Mechanisms and reactions during atomic layer deposition on polymers, *Coord. Chem. Rev.*, 2013, **257**, 3323–3331.

24 L. Konopasek and J. W. S. Hearle, Tensile fatigue behaviour of para-orientated aramid fibres and their fracture morphology, *J. Appl. Polym. Sci.*, 1977, **21**, 2791–2815.

25 Y. W. Mai and F. Castino, Fracture toughness of Kevlar-epoxy composites with controlled interfacial bonding, *J. Mater. Sci.*, 1984, **19**, 1638–1655.

26 A. R. Bunsell, The tensile and fatigue behaviour of Kevlar-49 (PRD-49) fibre, *J. Mater. Sci.*, 1975, **10**, 1300–1308.

27 L. Zhang, A. J. Patil, L. Li, A. Schierhorn, S. Mann, U. Gösele and M. Knez, Chemical infiltration during atomic layer deposition: metalation of porphyrins as model substrates, *Angew. Chem., Int. Ed.*, 2009, **48**, 4982–4985.

 This journal is © The Royal Society of Chemistry 2020